Egleide Y. Elenes
Mem. ASME
Department of Biomedical Engineering,
University of Texas at Austin,
301 E. Dean Keeton Street C2100,
Austin, TX 78712-2100
e-mail: eelenes@utexas.edu

Jason N. Mehta
Mem. ASME
Department of Mechanical Engineering,
University of Texas at Austin,
204 E. Dean Keeton Street,
Stop C2200,
Austin, TX 78712-1591
e-mail: jnmehta@utexas.edu

Fang-Chi Hsu
Department of Biostatistics and Data Science,
Division of Public Health Sciences,
Wake Forest Baptist Medical Center
Comprehensive Cancer Center,
1 Medical Center Boulevard,
Winston-Salem, NC 27157
e-mail: fhsu@wakehealth.edu

Christopher T. Whitlow
Department of Biostatistics and Data Science,
Division of Public Health Sciences,
Wake Forest School of Medicine,
Wake Forest Baptist Medical Center
Comprehensive Cancer Center,
1 Medical Center Boulevard,
Winston-Salem, NC 27157;
Department of Neurosurgery,
Wake Forest Baptist Medical Center,
1 Medical Center Boulevard,
Winston-Salem, NC 27157
e-mail: cwhitlow@wakehealth.edu

Waldermar Debinski
Wake Forest Baptist Medical Center
Comprehensive Cancer Center,
1 Medical Center Boulevard,
Winston-Salem, NC 27157
e-mail: debinski@wakehealth.edu

John Rossmeisl
School of Biomedical Engineering and Sciences,
Virginia Tech-Wake Forest University,
325 Kelly Hall, Stanger Street,
Blacksburg, VA 24061;
Virginia-Maryland Regional
College of Veterinary Medicine,
215 Duckpond Drive,
Virginia Tech,
Blacksburg, VA 24061
e-mail: jrossmeil@vt.edu

Stephen Tatter
Department of Neurosurgery,
Wake Forest Baptist Medical Center,
1 Medical Center Boulevard,
Winston-Salem, NC 27157
e-mail: statter@wakehealth.edu

Convection-Enhanced Arborizing Catheter System Improves Local/Regional Delivery of Infusates Versus a Single-Port Catheter in Ex Vivo Porcine Brain Tissue

Standard treatment for glioblastoma is noncurative and only partially effective. Convection-enhanced delivery (CED) was developed as an alternative approach for effective loco-regional delivery of drugs via a small catheter inserted into the diseased brain. However, previous CED clinical trials revealed the need for improved catheters for controlled and satisfactory distribution of therapeutics. In this study, the arborizing catheter, consisting of six infusion ports, was compared to a reflux-preventing single-port catheter. Infusions of iohexol at a flow rate of 1 μL/min/microneedle were performed, using the arborizing catheter on one hemisphere and a single-port catheter on the contralateral hemisphere of excised pig brains. The volume dispersed (V_d) of the contrast agent was quantified for each catheter. V_d for the arborizing catheter was significantly higher than for the single-port catheter, $2235.8 \pm 569.7\,mm^3$ and $382.2 \pm 243.0\,mm^3$, respectively ($n = 7$). Minimal reflux was observed; however, high V_d values were achieved with the arborizing catheter. With simultaneous infusion using multiple ports of the arborizing catheter, high V_d was achieved at a low infusion rate. Thus, the arborizing catheter promises a highly desirable large volume of distribution of drugs delivered to the brain for the purpose of treating brain tumors. [DOI: 10.1115/1.4048935]

Keywords: convection-enhanced delivery, volume dispersed, intracranial infusion, glioblastoma, drug delivery

Manuscript received February 28, 2020; final manuscript received July 19, 2020; published online December 2, 2020. Assoc. Editor: Ali Sadegh.

Christopher G. Rylander[1]
Department of Mechanical Engineering,
University of Texas at Austin,
204 E. Dean Keeton Street,
Stop C2200,
Austin, TX 78712-1591
e-mail: cgr@austin.utexas.edu

Introduction

Glioblastoma (GBM) is a high-grade malignant glioma with a mortality rate that exceeds 95% despite over eight decades of medical research dedicated to improve outcomes [1,2]. GBM is extremely difficult to treat in the brain and essentially incurable due to its complex pathobiology and highly infiltrative form [3]. The standard of care is complex, toxic, and invasive involving surgical resection [4], radiation [5], concomitant, and/or adjuvant chemotherapy [6,7]. Tumor recurrence is inevitable, typically recurring within a 1–2 cm vicinity of the original tumor site [8,9].

The blood brain barrier (BBB) and the blood brain tumor barrier (BBTB) form a major obstacle in malignant glioma therapy by hindering the delivery of sufficient quantities of potentially effective therapeutic agents [10,11]. A technique for loco-regional delivery known as convection-enhanced delivery (CED) demonstrated to be a viable approach for circumventing the BBB and BBTB. CED involves pressure-driven flow of therapeutics directly to the brain via a stereotactically guided small-caliber catheter [12,13]. Macromolecules are pumped primarily through the interstitial space of the brain parenchyma for a few hours or up to couple of weeks allowing greater distribution of molecules than obtained with simple diffusion [14,15]. Through local delivery of high concentrations of therapeutics directly to the diseased brain tissue, CED minimizes systemic and central nervous system toxicity.

Despite the promising results of CED in early clinical trials, it has yet to prove full clinical success. The interleukin 13 receptor alpha 2 (IL-13RA2) discovered to be overexpressed in GBM cells proved to be an attractive target in GBM [16–18]. The first generation of IL-13-based targeted cytotoxins, delivered via CED, increased patient survival by an average of 15 more weeks compared to median survival for these patients [19]. Propelled by the early favorable results, Phase III clinical trials (PRECISE trial) were conducted comparing CED of IL-13-PE38QQR and the Gliadel Wafer (a diffusion-based therapy approved by the Food and Drug Administration) in patients with recurrent GBM [20]. These trials failed to demonstrate statistically significant improvement in survival for the CED group compared to the control group. It is noteworthy to point out that to achieve the company's chosen clinical trial-endpoint, patients had to survive 50% longer than the historical controls. However, not a single drug in oncology has exhibited this kind of efficacy in this century [20]. An additional limitation of the study was that researchers used commercially available catheters designed for drug delivery into open liquid spaces, but not brain parenchyma or brain tumors. The catheters used appeared incapable of distributing drugs over large tissue volumes necessary for complete coverage of the tumor margins [21]. Thus, infiltrative GBM cells potentially residing in the primary tumor periphery (nonenhancing tumor), which correlate with tumor recurrence, were presumably left untreated [22].

The lack of CED-specific tools to perform the therapy in the PRECISE trial could have contributed to its disappointing results. The catheters used in the study had a single port for infusion, which are highly prone to air embolization and reflux, or backflow, along the catheter walls [23]. Hence, insertion of multiple single-port catheters was required to attempt larger distributions in the brain. The hazards of multiple insertion tracts include increased risk of trauma to healthy neurological tissue and greater probability of cell seeding healthy tissue with cancer cells along the insertion tracts [24,25]. Therefore, there is a clear clinical need for improved catheters that address the drug delivery limitations of CED [26].

Recognizing this need, catheters have been designed to incorporate a reflux-arresting property such as a "step change," in which the diameter of the catheter changes along the distal tip of the catheter [27–31]. In addition, Vogelbaum et al. have demonstrated that the Cleaveland Multiport Catheter successfully delivers a high volume of therapeutics during intra-and perioperative infusions in recurrent GBM and anaplastic astrocytoma [32]. The effectiveness of the Cleaveland Multiport Catheter supports the concept of utilizing multiple ports for achieving high volumes of dispersion, specifically in the nonenhancing, tumor-infiltrated brain tissue.

Our research group has developed the "arborizing catheter" to maximize drug dispersal in the brain [33,34]. The arborizing catheter consists of multiple infusion ports or "microneedles" originating from within a rigid cannula. This is an advantage over utilizing multiple single-port catheters because the arborizing catheter requires only one insertion path. Each microneedle individually arborizes (branches out) from the primary cannula to enhance drug delivery to desirable margins surrounding GBM. Risk of complications could be reduced because individual microneedles are ten-fold smaller than conventional catheters. In addition, the microneedles and all contact surfaces fully retract into the cannula during insertion and extraction of the catheter, thereby reducing the probability of tumor cell seeding in healthy brain tissue. The cannula–microneedle interface of the arborizing catheter is an inherent step change, which is a feature that has been demonstrated to mitigate reflux in the literature [29,35,36]. The disadvantage of the arborizing catheter design compared to single-port catheters is that multiple microneedles can increase the complexity of use and manufacturing.

We have previously demonstrated the greater volume dispersed (V_d) and mean distribution ratios (V_d:V_i) achieved with the arborizing catheter compared to single-port catheters in brain tissue phantoms [34]. In this study, we compare the performance of the arborizing catheter versus a single-port catheter in excised porcine brains.

Materials and Methods

Manufacturing of the Arborizing Catheter. The arborizing catheter was manufactured following the design specifications established through discussions within our group involving neurosurgeons (Table 1). The key feature of the catheter is the distal end of its primary cannula (3 mm outer diameter (OD)) that consists of biocompatible polyether ether ketone (PEEK) tubes (41568-L4, Analytical Sales & Services Inc., Flanders, NJ; OD 794 μm × inner diameter (ID) 381 μm) bent at a radius of curvature of 28.3 mm using a two-piece custom-manufactured fixture (Fig. 1(*a*)). Once arranged within the fixture, the PEEK tubes were fixed in their bent configuration with UV-cured medical grade adhesive (3972, Loctite®, Westlake, OH) (Fig. 1(*b*)).

[1]Corresponding author.

Following the curing process, the distal end of the cannula was polished to a smooth conical tip.

The PEEK tubes guide six microneedles made from small-gauge (OD 375 μm × ID 180 μm) fused-silica capillary fibers (TSP180375, General Separation Technologies, Newark, DE). Five microneedles were equally spaced surrounding the sixth microneedle at the center of the cannula. The distal end of each microneedle was cleaved flat. The proximal end of each microneedle was attached to a 22 G plastic dispensing needle with a Luer adapter that can quickly connect to small-bore extension tubing. The flexible, plastic dispensing needle was reinforced with PEEK tubing to add rigidity and prevent kinking/buckling during microneedle deployment.

Manufacturing of Single-Port Microneedle Catheter. The single-port catheters were modeled after commercially available, reflux-preventing step catheters (e.g., SmartFlow cannula, MRI Interventions Inc., Irvine, CA). The single-port catheter consisted of a single fused-silica capillary tube (i.e., microneedle) fixed inside PEEK tubing (OD 794 μm × ID 381 μm). To create the reflux-preventing step change, the PEEK-reinforced microneedle was inserted into a 1.5 mm-diameter OD PEEK tubing. The proximal end of each microneedle was attached to a 22 G plastic dispensing needle with a Luer adapter. The distal end of each microneedle was cleaved flat.

Two arborizing catheters and two single-port catheters were used for the infusion experiments in this study (Fig. 2(*a*)). When the microneedles are fully deployed, the small diameter of the microneedles interface with the larger diameter of the cannula to create a step change that helps arrest backflow (Fig. 2(*b*)). Similarly, the step change in the single-port catheter is demonstrated in the magnified image.

The fixture used to manufacture the arborizing catheter was designed to deflect the needles at 25 deg measured from the axis of the cannula. Images for each microneedle, deployed individually were taken and imported into IMAGE J (National Institutes of Health, Bethesda, MD) to measure the angle of deflection, θ (Fig. 2(*c*)). Transverse images of the distal tip of the cannula, with the microneedles fully deployed, were also taken to measure the angle between two adjacent microneedles, φ. The mean angle and standard deviation were 26.6 deg ± 1.2 deg and 72.0 deg ± 3.2 deg for θ and φ, respectively.

Specimen Preparation. Fresh commercial pig heads ($n = 7$) were procured from a local abattoir (Johnson City, TX) within hours of harvesting and processed at room temperature. To prevent X-ray attenuation during imaging due to excess tissue, the bulk of the head was removed leaving only a block of tissue encapsulating the cranium and brain (approximately 6 cm × 10 cm × 11 cm). An autopsy saw (Mopec, Oak Park, MI) was used to create a window in the outer table of the frontal bone overlying the sinus frontalis of the pigs. Two burr hole craniectomies, separated 1.5 cm apart, were then created in the inner table of the frontal bone providing access to each cerebral hemisphere.

Infusion Experiments. A custom-built fixture was used to hold the main cannula of the arborizing catheter and provide support to the microneedles to prevent them from buckling during deployment (Fig. 3(*a*)). The device consists of two plastic plates secured to a linear stage. The backplate contains vertical channels to help guide the microneedles and the front plate was used to effectively "sandwich" the catheter and microneedles, securing them to the linear stage. A second set of grips were used to secure the Luer locks of the microneedles to the translating portion of the linear stage. The single-port catheter and each microneedle of the arborizing catheter were connected to a fluid line and syringe via a three-way stopcock. Mountable gauge pressure sensors (PX26 series, Omega Engineering, Norwalk, CT) were connected to one port of the stopcock of each fluid line for each microneedle and for the single-port catheter. Pressure sensors numbered P1–P6 were assigned to each microneedle of the arborizing catheter and a seventh pressure sensor was assigned to the single-port catheter (Fig. 3(*b*)).

Before the catheters were inserted, the fluid lines for the single-port catheter and each microneedle were primed with the iodine-based imaging tracer, iohexol, with a concentration of 241.2 mg iodine/mL. The stopcock was closed to prevent fluid from escaping and the microneedles were fully retracted inside the cannula. The cannula of arborizing catheter and the single-port catheter were inserted manually, with the linear stage's micrometer, on the right and left hemispheres of the brain, respectively. The arborizing catheter was inserted approximately 1-cm deep from the brain surface. The single-port catheter was inserted approximately 2-cm deep from the brain surface. Both catheters were inserted at 40 deg using the flat surface of the tissue specimen as a reference.

A virtual graphical interface program written in LabVIEW (National Instruments, Austin, TX) was used to control a linear actuator (Zaber Technologies, Inc., Vancouver, BC) to simultaneously deploy the microneedles, 1-cm deep into brain tissue at an insertion rate of 0.33 mm/sec. The fluid lines were opened at the beginning of the insertion to allow flow and prevent clogging of the single-port catheter and microneedles during insertion into the tissue. The infusion flow rate was set to ramp from 0.5 to 1 μL/min/microneedle for the first 2 min, then to a constant flow rate of 1 μL/min/microneedle for the duration of infusion using a programmable syringe pump (Harvard Apparatus, Holliston, MA). The total infusion time was 4 h and 2 min. The flow rate was chosen based on clinically relevant flow rates for CED, which range from 0.5 to 10 μL/min [15,20,37–40]. In a seminal study, Bobo et al. investigated the distribution of two compounds administered to cat brains at a flow rate that increased from 0.5 to 4.0 μL/min [12]. The authors ascertained that stability was maintained throughout the infusion with no significant adverse effects [12]. Moreover, additional studies concluded that CED did not lead to cerebral edema [14].

Computed Tomography Imaging. Immediately following the infusion, the specimens were transported to the University of

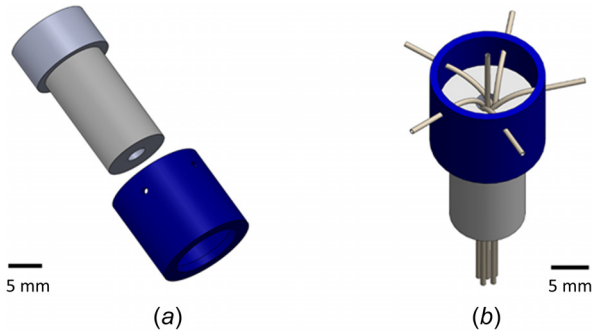

Fig. 1 (*a*) Drawing of the two components of the fixture for manufacturing the cannula of the arborizing catheter. (*b*) View of assembled fixture holding and bending the PEEK tubing in place for bonding.

Table 1 Design constraints and specifications for the arborizing catheter

Design criteria	Specification
Max cannula OD	3 mm
Length (for animal model)	13 cm
Max microneedle OD × ID	500 μm × 200 μm
Max microneedle deployment depth	5 cm
Number of ports	≥5
Microneedle separation distance	>1–1.5 cm
Materials	Ceramic, titanium, PEEK

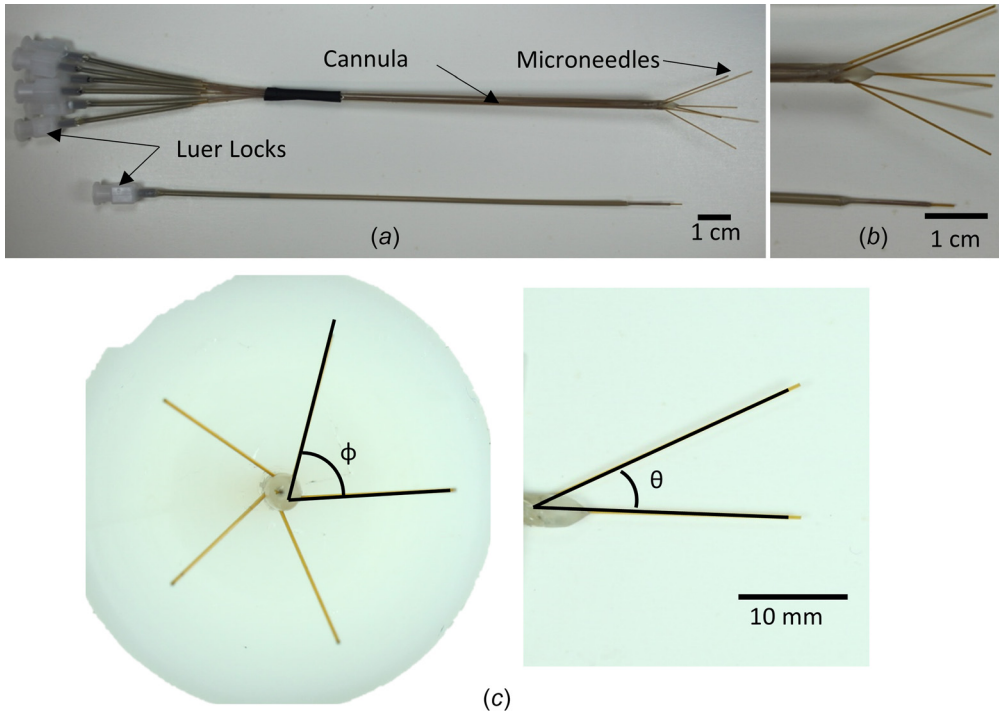

Fig. 2 (*a*) Image shows an arborizing catheter and single-port catheter. (*b*) Magnified image of distal ends of the catheters showing microneedle deflection in the arborizing catheter and the reflux-arresting step change for the respective catheters. (*c*) Measured angles for the arborizing catheter. Phi (φ) was defined as the angle along the axes of two adjacent needles. Theta (θ) was defined as the angle of deflection of each microneedle in reference to the axis of the cannula.

Texas at Austin high resolution X-ray computed tomography (CT) facility (UTCT) for CT scanning. Each specimen was imaged with the catheters in situ along with iohexol solution standards with concentrations ranging from 100% to 1% of the stock solution. All specimens were imaged with a North Star Imaging (Roger, MN) CT scanner and Perkin Elmer (Waltham, MA) detector. The specimens were scanned at 130 kV with a current of 0.13 mA. Voxel size was 133.3 μm for all three dimensions. The final image dataset ranged from 843 to 975 slices.

Image Analysis. For each specimen, stacks of 16-bit tag image file format images were imported into IMAGE J (NIH, Bethesda, MD) to extract the corresponding grayscale values from the iohexol solution calibration standards. The intensity value of each standard was averaged from 40 to 50 images. We selected 10% of the stock iohexol concentration as the threshold for calculating the volume dispersed (V_d) of the infusion. At this concentration, the mean grayscale intensity for the contrast agent was greater than that of the surrounding brain tissue.

After determining the average grayscale values for the solution standards and brain tissue, the image data was loaded into AVIZO (version 9.5 FEI Visualization Sciences Group, Hillsboro, OR) for volumetric segmentation. Each voxel size was defined as 133.3 μm for all three dimensions based on the CT images. The brain was isolated from the surrounding skull and superfluous tissue. Then a threshold range using the grayscale intensity value corresponding to the 10% stock concentration for the lower bound was applied to select the voxels corresponding to the infused contrast agent. This was done in three orthogonal views, leading to a three-dimensional preliminary "mask" containing the selected voxels. This original mask was sectioned into separate masks for each catheter. The infused volume on the right and left hemispheres corresponded to the arborizing catheter and the single-port catheter, respectively. Ventricular leakage was separated from the infusion volumes manually based on the structure of the lateral ventricles visualized in the images. Each catheter's individual contribution to ventricular leakage could not be clearly distinguished; thus, leakage was not subdivided, but rather aggregated into a single mask.

The material analysis function available in AVIZO was used to count each voxel and calculate the volume of each mask that represented V_d. Next, the masks corresponding to the single-port catheter, arborizing catheter, and ventricular leakage were exported from AVIZO as 16-bit tag image file format images. The mask and raw images were then imported into MATLAB (version 2018a Mathworks, Natick, MA). Closed voids in the infusion mask were filled using a flood-fill operation with pixel connectivity defined as horizontal, vertical, and diagonal adjacent pixels for each slice. Both the filled and unfilled masks were overlaid on the original raw files and grayscale intensity values were recorded for all areas within the infusion regions. The percent increase in number of voxels and the V_d for each new mask was calculated.

Given the prescribed flow rate and the infusion duration, the infused volume (V_i) per microneedle is known a priori, and was used to calculate the mean distribution ratio (V_d:V_i). Using MATLAB, a paired t-test for two paired samples was performed to analyze differences in V_d, V_d:V_i, and voxel percent increase for the two catheter groups assuming a significance level equal to 0.05. A Student's *t*-test was used to compare differences in V_d between the filled and unfilled masks.

In order to study spatial uniformity of the two catheters, grayscale intensity values for each mask were put into 20 bins ranging from 0 to 100% infusate concentration. Next, a ratio (percent voxels) was created for each bin by normalizing the data to the total number of voxels in each mask for each infusion. The mean, median, standard deviation, kurtosis, and skewness compare the histogram generated from the imaging data for each pig brain and specific catheter. These statistics could determine the shape of the histogram and were compared between the two catheters using a Wilcoxon rank sum test (analyzing one statistic at a time; ignoring

the dependency for the two histograms, one for each catheter, generated from the pig brain), multivariate analysis of variance (analyzing all statistics simultaneously), mixed effects models (considering the correlated structure), and generalized estimating equations (GEE) models (considering the correlated structure).

Additionally, the mixed effects models were used to examine the association between the two catheter groups and ratios after adjusting for concentration. Interactions between group and concentration in the model were included to explore whether the group effect on ratios changed by concentration level. Furthermore, using the 10% bin as the threshold concentration, any ratios below 10% or above 10% were considered as under or over saturated areas, respectively. Allowing some variation, a randomly selected cutoff point for the ratios (e.g., 15%, 20%, and 25%) was used to divide the ratios into two groups: (1) bad: less than 10% or greater than the selected cutoff point and (2) good: greater than or equal to 10% and less than or equal to the selected cutoff point. The GEE models with logit link and binomial distribution were used to study the association between groups and the dichotomized ratio. These analyses were performed using SAS statistical software (SAS Inc., Cary, NC).

Results

Following the infusion of iohexol into excised pig brains, specimens ($n = 7$) and vials of iohexol calibration standards were imaged with CT. Image stacks of the CT scan were imported into IMAGE J to quantify the grayscale intensity values for the solution dilutions that ranged from 1 to 100% concentration of the iohexol. The grayscale intensity values, averaged from 40 to 50 images, were plotted versus concentration of iohexol in an intensity–concentration calibration curve (Fig. 4).

The grayscale values derived from the calibration standards were used to set the grayscale threshold in AVIZO. Voxels corresponding to 10–100% concentration of infused iohexol were selected (Fig. 5(*a*)). The infusion volume from each hemisphere was further segmented into the single-port (displayed in blue) and arborizing catheter groups (displayed in red) (Fig. 5(*b*)). The ventricles of the brain acted as "low-pressure-sinks" and flow from the infusion solution leaked in and was labeled in its own category as "leakage" (displayed in green). For the majority of the specimens, the ventricles of the brain were filled with cerebrospinal fluid (CSF) and were indistinguishable from the surrounding tissue with grayscale thresholding. Therefore, the volume of infusion from each catheter was separated from the ventricular leakage manually and cutoff where flow tapered into the lateral ventricle (Fig. 5(*c*)). However, because the lateral ventricles are in communication with the third ventricle, it was not feasible to separate the contribution of ventricular leakage from each catheter.

The CT imaging revealed that in two specimens, one (labeled "specimen A") or two (labeled "specimen B") of the microneedles, from the arborizing catheter were not inserted into the brain parenchyma. Images showed that the microneedles were placed in the epidural space, or air pockets potentially caused by loss of CSF. This was taken into account when calculating V_d:$V_{i,}$ given the smaller total infused volume into the brain parenchyma due to needles not being inserted into the tissue for those two specimens.

A box plot demonstrating volume dispersed for the three groups: the arborizing catheter, single-port catheter, and ventricular leakage, is shown in Fig. 6(*a*). The outlier in the arborizing catheter group (defined outside the 1.5–times the interquartile range, below the lower quartile) corresponds to specimen B with two microneedles outside the brain tissue. V_d for the arborizing catheter ($2235.8 \pm 569.7\,mm^3$) was significantly higher ($p < 0.001$) than the V_d for the single-port catheter ($382.2 \pm 243.0\,mm^3$). Figure 6(*b*) shows a box plot comparing the mean distribution ratios for the arborizing catheter and the single-port catheter. Average values of V_d:V_i for the arborizing and single-port catheters were 1.6 ± 0.3 and 1.6 ± 1.0, respectively.

The closed void area for the single-port catheter corresponded to $0.67 \pm 0.52\%$ of the voxels in the filled mask, while it represented $1.60 \pm 1.01\%$ of the voxels in the filled mask for the arborizing catheter, yielding a noticeable, but not significant ($p = 0.067$) difference in void area. Table 2 shows a comparison of the volumes calculated for the filled and unfilled masks; no significant differences were found for either the single-port or the arborizing catheters. For the comparison of spatial uniformity between the two catheter groups, all statistical analyses showed that the histograms were similar between groups (all p-values > 0.05), as shown in Fig. 7. For examining the association between ratios and the catheter groups, the test was not statistically significant. This shows that there was no association between ratios and catheters. No matter what cutoff points were chosen for dichotomized ratios, the catheter groups were not associated with the dichotomized ratio. Overall, the ratios were not different between the single-port catheter and the arborizing catheter.

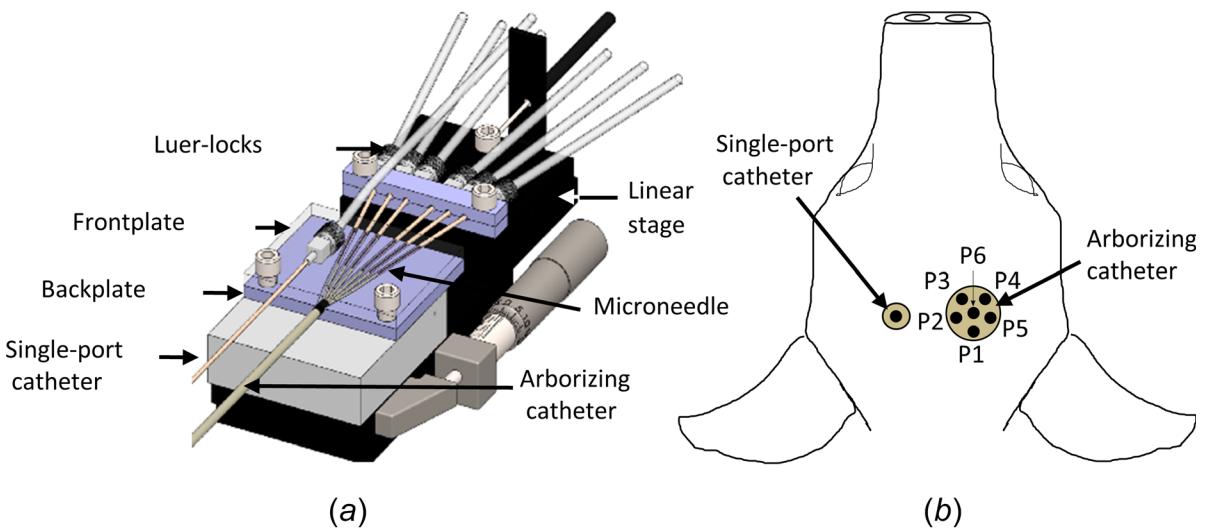

Fig. 3 (*a*) Diagram of fixture used to secure arborizing catheter and single-port catheter. The backplate and frontplate support and guide the microneedles (*b*) axial view of specimen demonstrating the arrangement of pressure sensors within each catheter. For the arborizing catheter, each dot represents the distal end of the microneedles fully deployed. Illustration not to scale.

Discussion

The design of the arborizing catheter aims to maximize V_d. Given the high recurrence rates of GBM [22,41], maximizing V_d is an approach to ensure that the peritumoral regions, frequently infiltrated by GBM cells, are treated. This means that local–regional "healthy" tissue would also be treated. Therefore, this treatment approach would complement targeted therapeutic agents with a wide therapeutic index to obviate peripheral damage of healthy brain tissue when designing for large V_d. Fortunately, the development of such suitable drugs has progressed significantly [2,42–44].

It was expected that the V_d from the arborizing catheter would be at least six times larger than for the single-port catheter given that V_i delivered for the catheter was six times greater. The actual difference in the V_d mean for the arborizing catheter was 5.8 times greater, practically achieving our expectations. The two specimens that did not have all six microneedles deployed in the brain parenchyma could explain the slightly lower value. Although consistency in positioning of the distal tip of the arborizing catheter's cannula within the tissue was the goal, the variability among the surface of the brains could have contributed to deviations. In some instances, there were air pockets between the surface of the brain and skull (i.e., subarachnoid space). Loss of perfusion, along with blood and CSF drainage due to the harvesting process, may be responsible for the formation of these air pockets. We observed flow of contrast agent through the subarachnoid space, especially for the specimens with microneedles near the surface of the brain. In specimens with needles between the folds of the brain, the contrast agent was pooled on the surface of the brain. This solution volume was not included as part of the infusion volume or ventricular leakage.

Specimen A with only five microneedles actively infusing in the brain resulted in V_d values comparable with V_d values for specimens with all six active microneedles. When dividing by the V_i expected for only five microneedles, its V_d:V_i was higher than the mean V_d:V_i (2.2 versus 1.6). However, specimen B with only four active microneedles in brain tissue demonstrated a notably smaller V_d (1070 mm^3), which in turn resulted in a small V_d:V_i. The small V_d for this specimen could be due to a compound effect of iohexol not infused in the brain tissue and loss due to leakage into the ventricle. However, that could not be confirmed because of the limitations with isolating leakage originating from the respective catheters. Another possibility is that in addition to two microneedles not being inserted in the brain, a third microneedle may have been clogged. The pressure data for microneedle labeled P2 in specimen B were saturated and stayed above the sensor's pressure range throughout the infusion (data not shown). When analyzing the CT images from Specimen B, we observed that minimal, if any, contrast enhancement was shown in the region where the P2 microneedle was inserted in the tissue. Thus, a total of 3/6 microneedles may have been inactive. Thus, if only half of the microneedles were active, the resultant V_d of 1070 mm^3 for Specimen B is expected because it is approximately half of the average V_d quantified for the arborizing group.

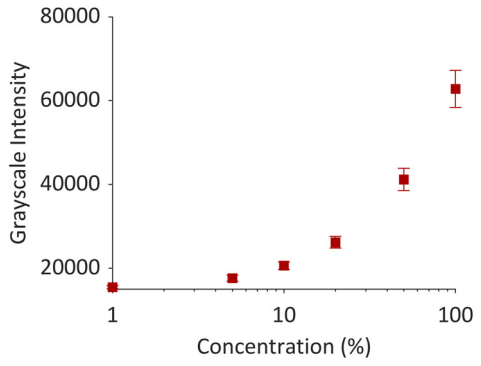

Fig. 4 Grayscale intensity values versus concentration. A concentration of 10% was selected for the lower bound grayscale threshold for selecting voxels of interest.

It is important to note that the V_d for the catheters is a mixture of the iohexol solution and interstitial fluid. Furthermore, the ventricular leakage is estimated from the iohexol mixing with the residual CSF after four hours of continuous infusion. Therefore, volumes for all three groups are notably larger than the total infused volume at 100% concentration. Lower leakage values were associated with larger V_d for the arborizing catheter and single-port catheter. A limitation of this study is that the excised brains were open systems and some of the CSF within the ventricles could have flowed out of the brain during the specimen preparation and/or experiments, which could influence the end results. The ventricles were filled with CSF for the majority of the specimens, but the contrast agent reached the base of the brain, and could have leaked out. However, we only were able to quantify the contrast agent left within the ventricles prior to imaging.

The flow rate of 1 μL/min was prescribed for each microneedle of the arborizing catheter and for the single-port catheter. The selected flow rate is on the low range of flow rates utilized in CED clinical trials and infusion studies. We were able to demonstrate that we can achieve high V_d, even at a low flow rate with the arborizing catheter. This is beneficial given that higher flow rates are associated with reflux [38,45]. In our study, we observed minimal reflux for both catheters, which was probably due to the step change incorporated in the catheters and the low flow rate selected.

Mean distribution ratios in this study were much lower than previous results in infusion experiments using agarose gel and similar flow rates [34,46]. Mean distribution ratios reported for the single-port catheter in agarose (at room temperature –24 °C) were 23.6 ± 2.1 and 15.0 ± 1.5 for the arborizing catheter, an order of magnitude larger than the results in this study. The differences can be expected due to the complex geometry and heterogeneous structure of the brain, which led to losses in solution due to ventricular leakage and leakage along the subarachnoid spaces. This highlights the challenges of CED for maximizing drug distribution in the brain. Due to the optically transparent nature of agarose gel, the minimum concentration for infused dyes could be orders of magnitude lower than the 10% minimum iohexol concentration that was needed for grayscale thresholding to segment the infusion volume in the CT scan. The inherent differences between agarose and brain tissue also stress the importance of performing infusion studies in brain tissue for the evaluation of our and other catheters. Although our specimens were excised tissue, V_d:V_i measured in this study were comparable to values measured in live canines and primate brains [41] and in rat brains [47].

The voxel percent increase due to void area was nearly significantly greater for the arborizing catheter. However, the voids do not significantly change the overall infusion volume. Nonetheless, any void presence is problematic for clinical treatment as any portion of the tumor not treated will create risk of tumor reoccurrence. The presence of increased void volume in the arborizing catheter may be due to the heterogeneous nature of the brain tissue rather than the design of the catheter. This could explain why, despite the increase in void volume with the arborizing catheter, both catheter groups had the same spatial distribution. This finding suggests minimal, yet sufficient, overlap by adjacent microneedles of the arborizing catheter creating a nearly contiguous concentrated infusion volume. Nonetheless, some techniques such as concurrent, nonlethal photothermal delivery with infusion, which has been shown to increase V_d by approximately 60–80% [47], may be beneficial in eliminating void volume. Additionally, intra-operative imaging may allow for early recognition of voids allowing for needle repositioning within the arborizing catheter to fill all void volumes in an efficient manner.

Because we were limited to imaging after the infusion was terminated, we could not decisively correlate the pressure spikes to adverse events such as lack of flow from a specific microneedle

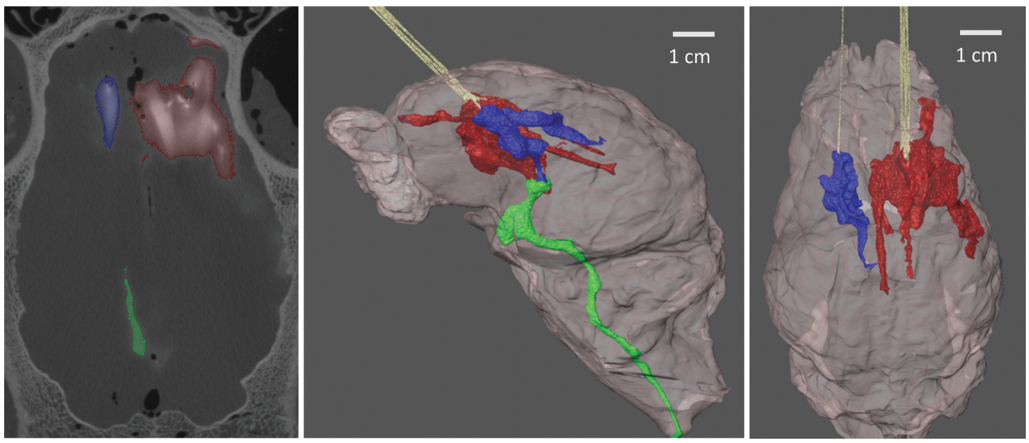

Fig. 5 Volumetric segmentation with AVIZO. (*a*) Voxels with grayscale value corresponding to ≥ 10% of iohexol concentration were selected to derive V_d for the single-port catheter (blue) and arborizing catheter (red). The volume of solution that leaked into the ventricles was segmented into a separate mask (green). (*b*) Volumetric rendering of the brain and V_d for each group. (*c*) Volumetric rendering showing infusion volumes for the single-port catheter and the arborizing catheter after removing ventricular leakage from image.

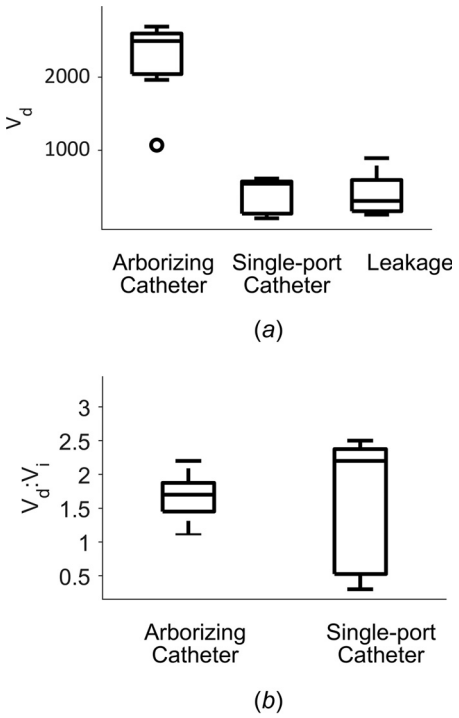

Fig. 6 (*a*) Box plot demonstrating dispersed volume (V_d) for the arborizing catheter, single-port catheter, and leakage of the contrast agent into the ventricles. The outlier corresponds to the specimen, which had two microneedles of the arborizing catheter outside of the brain tissue. (*b*) Box plot of mean distribution ratio (V_d:V_i) for the arborizing catheter and the single-port catheter.

due to possible clogging. Therefore, further exploration is required to find a concrete explanation for the higher pressures. One approach is to intermittently image the infusion in order to investigate the temporal distribution of the contrast agent, especially in the event of pressure spikes. The advantage of having multiple infusion ports is the individuality of shutoff or retraction

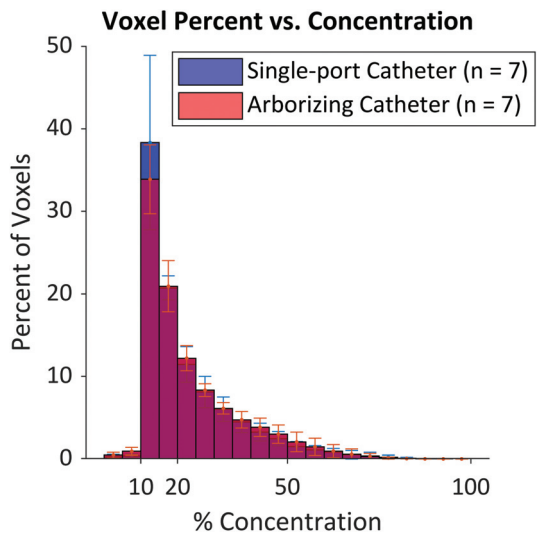

Fig. 7 Histogram of the voxel percent (ratio) against concentration percent where the blue section represents a larger average percent of voxels with the single-port catheter, the red represents the arborizing catheter having a larger average percent of voxels, and the purple is the overlap between the single-port catheter and the arborizing catheter

Table 2 Comparison of averaged V_d ± standard deviation (st dev) for masks with unfilled and filled closed voids

Catheter	Unfilled mask average V_d ± st dev (mm)	Filled mask average V_d±st dev (mm)	*P*-value
Single-port catheter	382.2 ± 243.0	385.4 ± 245.6	>0.99*
Arborizing catheter	2235.8 ± 569.7	2274.4 ± 590.2	>0.99*

**p* value calculated using a two-sample *t*-test.

control for each of the microneedles in the event of an adverse effect or in an attempt to dislodge clogged tissue, respectively.

Conclusions

We demonstrated the greater performance of the arborizing catheter versus a step single-port catheter with infusions of iohexol in excised pig brains. Following the infusions, CT scans of the brains were taken and AVIZO was used to analyze the images and quantify V_d of the infused contrast agent. Volume dispersed for the arborizing catheter was significantly higher (5.8 times higher) than the V_d achieved with the single-port catheter. The high V_d values were achieved at a slow flow rate that resulted in minimal reflux for either catheter. Mean distribution ratios for both catheters were not significantly different. The greater V_d achieved with the arborizing catheter are beneficial for maximizing drug coverage of the intended tumor and tumor margin target volume and potentially improving the efficacy of CED.

Acknowledgment

The authors would like to thank Dr. Matthew Colbert, David Edey, and Dr. Jessie Maisano at UTCT for their help scanning specimens and access to AVIZO software. The authors also thank Yousef S. Ahmad for his help with data analysis.

Funding Data

- National Institutes of Health/National Cancer Institute (NIH/NCI) (Grant No. P01 CA207206-01; Funder ID: 10.13039/100000002 and 10.13039/100000054).

Nomenclature

CED = convection enhanced delivery
cm = centimeter
CSF = cerebral spinal fluid
CT = computed tomography
G = gage
GBM = glioblastoma
GEE = generalized estimating equations
ID = inner diameter
mg = milligram
ml = milliliter
MRI = magnetic resonance imaging
OD = outer diameter
PEEK = polyether ether ketone
UV = ultra violet
V_d = volume dispersed
V_d:V_i = mean distribution ratio
V_i = volume infused

References

[1] Ostrom, Q. T., Gittleman, H., Xu, J., Kromer, C., Wolinsky, Y., Kruchko, C., and Barnholtz-Sloan, J. S., 2016, "CBTRUS Statistical Report: Primary Brain and Other Central Nervous System Tumors Diagnosed in the United States in 2009-2013," Neuro Oncol., **18**(suppl_5), pp. v1–v75.

[2] Debinski, W., Priebe, W., and Tatter, S. B., 2017, *Maximizing Local Access to Therapeutic Deliveries in Glioblastoma. Part I: Targeted Cytotoxic Therapy*, S. De Vleeschouwer Glioblastoma, ed., Codon Publications, Brisbane, Australia, pp. 341–358.

[3] Nishikawa, R., 2010, "Standard Therapy for Glioblastoma—A Review of Where We Are," Neurol. Med. Chir. (Tokyo), **50**(9), pp. 713–719.

[4] Sanai, N., and Berger, M. S., 2012, "Recent Surgical Management of Gliomas," *Glioma: Immunotherapeutic Approaches*, R. Yamanaka, ed., Springer, New York, pp. 12–25.

[5] Chan, M. D., Tatter, S. B., Lesser, G., and Shaw, E. G., 2010, "Radiation Oncology in Brain Tumors: Current Approaches and Clinical Trials in Progress," Neuroimaging Clin. North Am., **20**(3), pp. 401–408.

[6] Lesser, G. J., and Grossman, S., 1994, "The Chemotherapy of High-Grade Astrocytomas," Semin. Oncol., **21**(2), pp. 220–235.

[7] Stupp, R., Mason, W. P., van den Bent, M. J., Weller, M., Fisher, B., Taphoorn, M. J., Belanger, K., Brandes, A. A., Marosi, C., Bogdahn, U., Curschmann, J., Janzer, R. C., Ludwin, S. K., Gorlia, T., Allgeier, A., Lacombe, D., Cairncross, J. G., Eisenhauer, E., and Mirimanoff, R. O., 2005, "Radiotherapy Plus Concomitant and Adjuvant Temozolomide for Glioblastoma," N. Engl. J. Med., **352**(10), pp. 987–996.

[8] Chen, L., Chaichana, K. L., Kleinberg, L., Ye, X., Quinones-Hinojosa, A., and Redmond, K., 2015, "Glioblastoma Recurrence Patterns Near Neural Stem Cell Regions," Radiother. Oncol., **116**(2), pp. 294–300.

[9] Wallner, K. E., Galicich, J. H., Krol, G., Arbit, E., and Malkin, M. G., 1989, "Patterns of Failure Following Treatment of Glioblastoma Multiforme and Anaplastic Astrocytoma," Int. J. Radiat. Oncol. Biol. Phys., **16**(6), pp. 1405–1409.

[10] Groothuis, D. R., 2000, "The Blood-Brain and Blood-Tumor Barriers: A Review of Strategies for Increasing Drug Delivery," Neuro Oncol., **2**(1), pp. 45–59.

[11] van Tellingen, O., Yetkin-Arik, B., de Gooijer, M. C., Wesseling, P., Wurdinger, T., and de Vries, H. E., 2015, "Overcoming the Blood-Brain Tumor Barrier for Effective Glioblastoma Treatment," Drug Resist. Updat., **19**, pp. 1–12.

[12] Bobo, R. H., Laske, D. W., Akbasak, A., Morrison, P. F., Dedrick, R. L., and Oldfield, E. H., 1994, "Convection-Enhanced Delivery of Macromolecules in the Brain," Proc. Natl. Acad. Sci. U. S. A., **91**(6), pp. 2076–2080.

[13] Morrison, P. F., Laske, D. W., Bobo, H., Oldfield, E. H., and Dedrick, R. L., 1994, "High-Flow Microinfusion: Tissue Penetration and Pharmacodynamics," Am. J. Physiol., **266**(1), pp. R292–R305.

[14] Vandergrift, W. A., Patel, S. J., Nicholas, J. S., and Varma, A. K., 2006, "Convection-Enhanced Delivery of Immunotoxins and Radioisotopes for Treatment of Malignant Gliomas," Neurosurg. Focus, **20**(4), p. E13.

[15] Laske, D. W., Youle, R. J., and Oldfield, E. H., 1997, "Tumor Regression With Regional Distribution of the Targeted Toxin TF-CRM107 in Patients With Malignant Brain Tumors," Nat. Med., **3**(12), pp. 1362–1368.

[16] Debinski, W., Obiri, N. I., Powers, S. K., Pastan, I., and Puri, R., 1995, "Human Glioma Cells Overexpress Receptors for Interleukin 13 and Are Extremely Sensitive to a Novel Chimeric Protein Composed of Interleukin 13 and Pseudomonas Exotoxin," Clin. Cancer Res., **1**, pp. 1253–1258.

[17] Debinski, W., Gibo, D., Hulet, S. W., Connor, J. R., and Gillespie, G. Y., 1999, "Receptor for Interleukin 13 is a Marker and Therapeutic Target for Human High-Grade Gliomas," Clin. Cancer Res., **5**, pp. 985–990.

[18] Debinski, W., Obiri, N. I., Pastan, I., and Puri, R. K., 1995, "A Novel Chimeric Protein Composed of Interleukin 13 and Pseudomonas Exotoxin is Highly Cytotoxic to Human Carcinoma Cells Expressing Receptors for Interleukin 13 and Interleukin 4," J. Biol. Chem., **270**(28), pp. 16775–16780.

[19] Kunwar, S., Prados, M. D., Chang, S. M., Berger, M. S., Lang, F. F., Piepmeier, J. M., Sampson, J. H., Ram, Z., Gutin, P. H., Gibbons, R. D., Aldape, K. D., Croteau, D. J., Sherman, J. W., Puri, R. K., and Cintredekin Besudotox Intraparenchymal Study, G., 2007, "Direct Intracerebral Delivery of Cintredekin Besudotox (IL13-PE38QQR) in Recurrent Malignant Glioma: A Report by the Cintredekin Besudotox Intraparenchymal Study Group," J. Clin. Oncol., **25**(7), pp. 837–844.

[20] Kunwar, S., Chang, S., Westphal, M., Vogelbaum, M., Sampson, J., Barnett, G., Shaffrey, M., Ram, Z., Piepmeier, J., Prados, M., Croteau, D., Pedain, C., Leland, P., Husain, S. R., Joshi, B. H., Puri, R. K., and PRECISE Study Group, 2010, "Phase III Randomized Trial of CED of IL13-PE38QQR vs Gliadel Wafers for Recurrent Glioblastoma," Neuro Oncol., **12**(8), pp. 871–881.

[21] Sampson, J. H., Archer, G., Pedain, C., Wembacher-Schröder, E., Westphal, M., Kunwar, S., Vogelbaum, M. A., Coan, A., Herndon, J. E., Raghavan, R., Brady, M. L., Reardon, D. A., Friedman, A. H., Friedman, H. S., Rodríguez-Ponce, M. I., Chang, S. M., Mittermeyer, S., Croteau, D., Puri, R. K., and PRECISE Trial Investigators, 2010, "Poor Drug Distribution as a Possible Explanation for the Results of the PRECISE Trial," J. Neurosurg., **113**(2), pp. 301–309.

[22] Hochberg, F. H., and Pruitt, A., 1980, "Assumptions in the Radiotherapy of Glioblastoma," Neurology, **30**(9), pp. 907–911.

[23] Lonser, R. R., Sarntinoranont, M., Morrison, P. F., and Oldfield, E. H., 2015, "Convection-Enhanced Delivery to the Central Nervous System," J. Neurosurg., **122**(3), pp. 697–706.

[24] Schwartz, H. S., and Spengler, D. M., 1997, "Needle Tract Recurrences After Closed Biopsy for Sarcoma: Three Cases and Review of the Literature," Ann. Surg. Oncol., **4**(3), pp. 228–236.

[25] Denton, K. J., Cotton, D. W., Nakielny, R. A., and Goepel, J. R., 1990, "Secondary Tumour Deposits in Needle Biopsy Tracks: An Underestimated Risk?," J. Clin. Pathol., **43**(1), pp. 83–83.

[26] Debinski, W., and Tatter, S. B., 2009, "Convection-Enhanced Delivery for the Treatment of Brain Tumors," Exp. Rev. Neurother., **9**(10), pp. 1519–1527.

[27] Brady, M. L., Raghavan, R., Singh, D., Anand, P. J., Fleisher, A. S., Mata, J., Broaddus, W. C., and Olbricht, W. L., 2014, "In Vivo Performance of a Microfabricated Catheter for Intraparenchymal Delivery," J. Neurosci. Meth., **229**, pp. 76–83.

[28] Gill, T., Barua, N. U., Woolley, M., Bienemann, A. S., Johnson, D. E., Sullivan, S. O., Murray, G., Fennelly, C., Lewis, O., Irving, C., Wyatt, M. J., Moore, P., and Gill, S. S., 2013, "In Vitro and In Vivo Testing of a Novel Recessed-Step Catheter for Reflux-Free Convection-Enhanced Drug Delivery to the Brain," J. Neurosci. Meth., **219**(1), pp. 1–9.

[29] Krauze, M. T., Saito, R., Noble, C., Tamas, M., Bringas, J., Park, J. W., Berger, M. S., and Bankiewicz, K., 2005, "Reflux-Free Cannula for Convection-Enhanced High-Speed Delivery of Therapeutic Agents," J. Neurosurg., **103**(5), pp. 923–929.

[30] Vazquez, L. C., Hagel, E., Willenberg, B. J., Dai, W., Casanova, F., Batich, C. D., and Sarntinoranont, M., 2012, "Polymer-Coated Cannulas for the Reduction of Backflow During Intraparenchymal Infusions," J. Mater. Sci. Mater. Med., **23**(8), pp. 2037–2046.

[31] Yin, D., Forsayeth, J., and Bankiewicz, K. S., 2010, "Optimized Cannula Design and Placement for Convection-Enhanced Delivery in Rat Striatum," J. Neurosci. Meth., **187**(1), pp. 46–51.
[32] Vogelbaum, M. A., Brewer, C., Barnett, G. H., Mohammadi, A. M., Peereboom, D. M., Ahluwalia, M. S., and Gao, S., 2018, "First-in-Human Evaluation of the Cleveland Multiport Catheter for Convection-Enhanced Delivery of Topotecan in Recurrent High-Grade Glioma: Results of Pilot Trial 1," J. Neurosurg., pp. 1–10.
[33] Andriani, R. T., 2014, *Design and Validation of Medical Devices for Photothermally Augmented Treatments*, Virginia Tech, Blacksburg, VA.
[34] Elenes, E. Y., and Rylander, C. G., 2017, *Maximizing Local Access to Therapeutic Deliveries in Glioblastoma. Part II: Arborizing Catheter for Convection-Enhanced Delivery in Tissue Phantoms*, S. De Vleeschouwer Glioblastoma, ed., Codon Publications, Brisbane, Australia.
[35] Fiandaca, M. S., Forsayeth, J. R., Dickinson, P. J., and Bankiewicz, K. S., 2008, "Image-Guided Convection-Enhanced Delivery Platform in the Treatment of Neurological Diseases," Neurotherapeutics, **5**(1), pp. 123–127.
[36] Vogelbaum, M. A., and Aghi, M. K., 2015, "Convection-Enhanced Delivery for the Treatment of Glioblastoma," Neuro Oncol., **17**(Suppl. 2), pp. ii3–ii8.
[37] Sampson, J. H., Akabani, G., Archer, G. E., Bigner, D. D., Berger, M. S., Friedman, A. H., Friedman, H. S., Herndon Ii, J. E., Kunwar, S., Marcus, S., McLendon, R. E., Paolino, A., Penne, K., Provenzale, J., Quinn, J., Reardon, D. A., Rich, J., Stenzel, T., Tourt-Uhlig, S., Wikstrand, C., Wong, T., Williams, R., Yuan, F., Zalutsky, M. R., and Pastan, I., 2003, "Progress Report of a Phase I Study of the Intracerebral Microinfusion of a Recombinant Chimeric Protein Composed of Transforming Growth Factor (TGF)-A and a Mutated Form of the Pseudomonas Exotoxin Termed PE-38 (TP-38) for the Treatment of Malignant Brain Tumors," J. Neurooncol., **65**(1), pp. 27–35.
[38] Chen, M. Y., Lonser, R. R., Morrison, P. F., Governale, L. S., and Oldfield, E. H., 1999, "Variables Affecting Convection-Enhanced Delivery to the Striatum: A Systematic Examination of Rate of Infusion, Cannula Size, Infusate Concentration, and Tissue–Cannula Sealing Time," J. Neurosurg., **90**(2), pp. 315–320.
[39] Rand, R. W., Kreitman, R. J., Patronas, N., Varricchio, F., Pastan, I., and Puri, R. K., 2000, "Intratumoral Administration of Recombinant Circularly Permuted Interleukin-4-Pseudomonas Exotoxin in Patients With High-Grade Glioma," Clin. Cancer Res., **6**(6), pp. 2157–2165.
[40] Patel, S. J., Shapiro, W. R., Laske, D. W., Jensen, R. L., Asher, A. L., Wessels, B. W., Carpenter, S. P., and Shan, J. S., 2005, "Safety and Feasibility of Convection-Enhanced Delivery of Cotara for the Treatment of Malignant Glioma: Initial Experience in 51 Patients," Neurosurgery, **56**(6), pp. 1243–1253.
[41] Varenika, V., Dickinson, P., Bringas, J., LeCouteur, R., Higgins, R., Park, J., Fiandaca, M. S., Berger, M., Sampson, J., and Bankiewicz, K., 2008, "Detection of Infusate Leakage in the Brain Using Real-Time Imaging of Convection-Enhanced Delivery," J. Neurosurg., **109**(5), pp. 874–880.
[42] Polivka, J., Jr., Polivka, J., Holubec, L., Kubikova, T., Priban, V., Hes, O., Pivovarcikova, K., and Treskova, I., 2017, "Advances in Experimental Targeted Therapy and Immunotherapy for Patients With Glioblastoma Multiforme," Anticancer Res., **37**(1), pp. 21–33.
[43] Touat, M., Idbaih, A., Sanson, M., and Ligon, K. L., 2017, "Glioblastoma Targeted Therapy: Updated Approaches From Recent Biological Insights," Ann. Oncol., **28**(7), pp. 1457–1472.
[44] Xu, Y. Y., Gao, P., Sun, Y., and Duan, Y. R., 2015, "Development of Targeted Therapies in Treatment of Glioblastoma," Cancer Biol. Med., **12**(3), pp. 223–237.
[45] Morrison, P. F., Chen, M. Y., Chadwick, R. S., Lonser, R. R., and Oldfield, E. H., 1999, "Focal Delivery During Direct Infusion to Brain: Role of Flow Rate, Catheter Diameter, and Tissue Mechanics," Am. J. Physiol., **277**(4), pp. R1218–R1229.
[46] Hood, R. L., Andriani, R. T., Ecker, T. E., Robertson, J. L., and Rylander, C. G., 2015, "Characterizing Thermal Augmentation of Convection-Enhanced Drug Delivery With the Fiberoptic Microneedle Device," Engineering, **1**(3), pp. 344–350.
[47] Hood, R. L., Andriani, R. T., Jr., Emch, S., Robertson, J. L., Rylander, C. G., and Rossmeisl, J. H., Jr., 2013, "Fiberoptic Microneedle Device Facilitates Volumetric Infusate Dispersion During Convection-Enhanced Delivery in the Brain," Lasers Surg. Med., **45**(7), pp. 418–426.